Dynamic radiometric calibration and radiometric matching of multiple microbolometer detector arrays

Hagen, Nathan

Nathan Hagen, "Dynamic radiometric calibration and radiometric matching of multiple microbolometer detector arrays," Proc. SPIE 11502, Infrared Remote Sensing and Instrumentation XXVIII, 115020M (20 August 2020); doi: 10.1117/12.2567811

SPIE.

Event: SPIE Optical Engineering + Applications, 2020, Online Only

Dynamic radiometric calibration and radiometric matching of multiple microbolometer detector arrays

Nathan Hagen

Utsunomiya University, Department of Optical Engineering, Center for Optical Research and Engineering (CORE), Utsunomiya, Tochigi 321-8585 Japan

ABSTRACT

While uncooled microbolometer cameras have made infrared imaging accessible to a much wider range of applications than their cryo-cooled competitors, they are notorious for having poor noise performance and problems with calibration drift. The drift causes microbolometer cameras to lose radiometric accuracy over time, and this is a serious problem for radiometrically combining multiple detector arrays because the drift is not the same for each camera, and existing calibration methods cannot adequately compensate for it. We show methods to dynamically correct for calibration drift during measurements, so that multiple detector arrays can be kept in radiometric agreement with one another.

Keywords: infrared imaging, calibration, drift, microbolometer, radiometry

1. INTRODUCTION

Uncooled microbolometer detector arrays are a convenient and low-cost approach to thermal imaging, but are notorious for having high noise, sensitivities that vary from pixel to pixel, and for calibration drift. In order to calibrate the pixel-dependent sensitivities, the traditional approach is to block the camera's field of view with a uniform-temperature shutter (temperature T_{cool}) followed by a second uniform-temperature shutter (temperature T_{warm}). With these two reference images, we can easily caclulate the appropriate offset and gain values at each pixel (as in Sec. 2 below). However, as soon as the calibration is complete, and the shutters open to reveal the scene to the sensor, the calibration parameters immediately start to change, as the detector array, camera housing, and lens change in temperature. While the changes are gradual, a recalibration every couple of minutes is generally needed in order to compensate for the drift in the calibration paremeters.

A number of researchers have tried to improve on this situation. Parrish and Woolaway modified the calibration procedure to create a different set of calibration parameters for a range of detector array temperatures.[1] By using a temperature sensor placed on the FPA itself, we can select the appropriate calibration set to fit the current state. Indeed, something like this is basically implemented on all commercial microbolometer cameras today, though the correction is typically only applied to the gain parameters. A similar approach, refined to provide more fine-grained correction has been implemented by Nugent *et al.* and Liang *et al.*[2,3] Other researchers have tried alternative system architectures, such as replacing the opaque shutter with a partially-transparent, partially-reflecting shutter,[4] or with a spherical mirror having a central hole.[5]

While these methods have interesting new properties, and some improve the current state of affairs, my own experience has been that these methods still have trouble maintaining absolute radiometric accuracy to much better than about 1 °C. That is, if we use two microbolometer cameras, corrected with the above methods, viewing the same scene, the cameras can achieve consistent agreement about the scene radiance temperatures to within about 1 °C. One also finds that, despite the attempts at drift correction, the correction is not quite consistent. Even if the cameras are forced to match one another during an initial calibration, they will immediately start to drift apart during operation, on the scale of tens of millidegrees in just a few seconds. In fact, this problem of achieving accurate radiometric matching of microbolometer cameras has been considered to be so intractable that a number of experts have given it up as hopeless.

In the discussion below, we show that, while tricky, it is not at all a hopeless problem, and we show how to modify an array of microbolometer cameras such that radiometric matching can be achieved. We start by reviewing the "static calibration" achieved using a pair of shutters. If the bulk of the error can be considered as a scalar offset across the entire array (that is, we need not consider pixel-to-pixel variations, for short term periods) then we can achieve the same effect by placing two reference blackbodies into the scene itself. Any change in the reference blackbodies within the scene can be approximated as global changes to the entire FPA, such that forcing the cameras to agree on the radiance temperatures

Infrared Remote Sensing and Instrumentation XXVIII, edited by Marija Strojnik,
Proceedings of SPIE Vol. 11502, 115020M · © 2020 SPIE
CCC code: 0277-786X/20/$21 · doi: 10.1117/12.2567811

of the blackbodies effectively brings them into radiometric matching. Inserting reference blackbodies into every scene to be measured is impractical, but if we block a portion of each camera's field of view, we can place a reference source into the blocked region, and this can be maintained quite close to the camera. With multiple cameras all viewing the same reference sources, it becomes possible to maintain radiometric matching of multiple detector arrays to within about 4×NETD despite the problems of detector drift, for several minutes. After several minutes, pixel-dependent variations start to become intolerably large, so that renewed static calibrations, or corrections such as those discussed in Refs 2, 3 become necessary to maintain radiometric matching.

2. STATIC CALIBRATION OF MICROBOLOMETER CAMERA IMAGES

The measurement g, in units of digital counts, at a given pixel can be approximated by[6]

$$g = \alpha + \gamma_0 A_{\text{pix}}\, \Omega \int R(\lambda)\, \tau(\lambda)\, L_{\text{obj}}(\lambda)\, d\lambda\,, \tag{1}$$

where $L(\lambda)$ is the object radiance spectrum, A_{pix} is the pixel area, Ω is the solid angle of the lens exit pupil as viewed by the pixel, R is the detector responsivity, and τ is the optical transmission. The "offset" and "gain" parameters of the camera are represented by α and γ_0. The detector element also receives light from the surrounding background (such as the camera housing), but this can be subsumed into an offset term that varies with camera temperature, $\alpha(T_{\text{cam}})$. The responsivity and the optical transmission also have some temperature dependence, which we can represent as $\gamma_0(T_{\text{cam}}, T_{\text{fpa}})$. Here T_{cam} is the averaged temperature of the camera housing, and T_{fpa} is the temperature of the focal plane array itself.

Taking the radiance-spectrum weighted averages of the responsivity and optical transmission, (1) becomes

$$g = \alpha + \gamma_0 A_{\text{pix}}\, \Omega\, \Delta\lambda\, \bar{R}\bar{\tau}\bar{L} = \alpha + \gamma_1 \bar{L}\,, \tag{2}$$

where overbars indicate an average, and the various object-independent parameters have been subsumed inside the new gain parameter γ_1. If the scene object temperatures do not occupy a wide range, then we can approximate the radiance as a linear function of temperature, and the radiance-based measurement equation of (2) can be approximated with a temperature-based one:

$$g \approx \alpha + \gamma T_{\text{obj}}\,. \tag{3}$$

Although the radiance-based method is more accurate, we will use the temperature-based equation below in order to keep the discussion as simple as possible.

The offset and gain are unknown parameters that must be calibrated. In order to determine their values, we can place two blackbody objects of different temperatures in front of the camera, and measure the response to each, and solve for α and γ. If we designate the cooler object temperature as T_{cool} and the warmer object temperature as T_{warm}, then the measurements at each pixel can be written as

$$\begin{aligned} g_{\text{cool}} &= \alpha + \gamma\big(T_{\text{cool}} - T_{\text{cool}}\big)\,, \\ g_{\text{warm}} &= \alpha + \gamma\big(T_{\text{warm}} - T_{\text{cool}}\big)\,. \end{aligned}$$

From these, we see that the offset value is simply $\alpha = g_{\text{cool}}$ (the measured pixel value in counts when viewing the cool reference), and the gain value γ in counts/°C as

$$\gamma = \frac{g_{\text{cool}} - g_{\text{warm}}}{T_{\text{cool}} - T_{\text{warm}}}\,. \tag{4}$$

Thus, if a pixel measures $g_{\text{cool}} = 7000$ and $g_{\text{warm}} = 5000$ for objects at temperatures $T_{\text{cool}} = 20\,°\text{C}$ and $T_{\text{warm}} = 30\,°\text{C}$, then the estimated offset and gain values will be $\alpha = 5000\,\text{cts}$ and $\gamma = 200\,\text{cts}/°\text{C}$.

We convert the raw pixel value g for any scene (in units of counts) to estimated radiance temperature $\hat{T}$ with

$$\hat{T} = \frac{1}{\gamma}(g - \alpha) + T_{\text{cool}}\,. \tag{5}$$

This is the conventional "nonuniformity correction" (NUC). Since the α and γ parameters do not change from one calibration to the next, we will refer to them together as the "static calibration".

3. DYNAMIC CALIBRATION

After the static calibration is complete, we raise the camera shutter and expose the detector array to the scene. First we consider placing two blackbodies into the scene, where T_{cool} and T_{warm} are their temperatures as estimated by the camera, while W_{cool} and W_{warm} are the *a priori* known blackbody temperatures. In practice, we can use thermisters on the blackbodies to tell us W. For radiometric matching of cameras, we can alternatively use one cameras as a "reference" camera, and force all of the other cameras viewing the blackbody references to match to it. This latter method maintains matching between cameras but sacrifices absolute radiometry.

The largest part of the calibration drift is the same for all pixels, and so we can use the pixels that view the reference blackbodies to correct the pixels viewing the remainder of the scene. Thus, the dynamic calibration gives a corrected temperature T' from the initial temperature T estimated at each pixel in a camera using

$$T'(x, y) = \omega + \beta\, T(x, y), \tag{6}$$

where

$$\omega = W_{\text{cool}} - \beta T_{\text{cool}}$$

is the dynamic offset correction factor, and

$$\beta = \frac{W_{\text{warm}} - W_{\text{cool}}}{T_{\text{warm}} - T_{\text{cool}}}$$

is the dynamic gain correction factor. These are "dynamic" because they are estimated and applied to correct each measurement frame. As a check, we can substitute T_{cool} for T in (6) and verify that we get the result $T' = W_{\text{cool}}$. Likewise, substituting T_{warm} into T gives $T' = W_{\text{warm}}$, as we expect. In addition, if we have only one reference blackbody in the scene rather than two, then we can apply an offset-only dynamic correction by setting $\beta = 1$.

While applying the dynamic correction (6) is straightforward and the procedure is simple enough to apply to a video stream coming from a high-resolution camera, placing reference blackbodies into each scene is impractical. We need a means of putting the reference sources into the camera's field of view while keeping them close to the camera body itself. To do this, we can construct an aperture that obstructs the cameras' field of view, as in Fig. 1. If we ignore for the moment the fact that these reference sources will be out of focus, then we can place an array of blackbody sources around the edge of the aperture, and these will be visible at the edges of the cameras' fields of view. Using film-based heater elements and thermisters, we can coat the emitting surface of these reference sources to give high emissivity, and control their temperatures to give inputs for W_{cool} and W_{warm}.

While each of the reference sources of Fig. 1 can be independently controlled, it is difficult to get all of the various thermisters to agree with one another. Since each camera will generally see not only its own pair of reference sources but also one of the adjacent camera's reference sources, this overlap can be use to improve agreement among the cameras. However, radiometric matching of the cameras is still not ideal.

In order to improve the matching of cameras, we would like all of the cameras to be looking at the *same* reference blackbody sources. In order to make this possible, we can replace the array of reference sources placed along the external aperture with an array of imaging mirrors, designed to relay the image of the two reference sources into each camera's respective field of view. The resulting layout is shown in Fig. 2. A convenient location for placing the reference sources is in the interstitial space between the cameras, so that the re-imaging mirrors need not have a severe tilt angle.

4. VIEW OBSTRUCTION AND BLURRING

Because we are placing the reference sources at a short dictance in front of the camera lens, their image will be blurry at the detector array. This by itself is not a problem, since there is no need to spatially resolve the references — we need only average the temperature that we measure across the face of the blackbody. However, the blurring means that we need to allow enough margin so that the temperature profile of the scene does not blur into the image of the reference source. In the case of Fig. 2, where the mirrors are imaging the sources onto the detector arrays, the images of the blackbodies will be in focus, but the mirrors themselves will be out of focus. As a result, the margin that we need to allow is the same for both cases (Fig. 1 and Fig. 2).

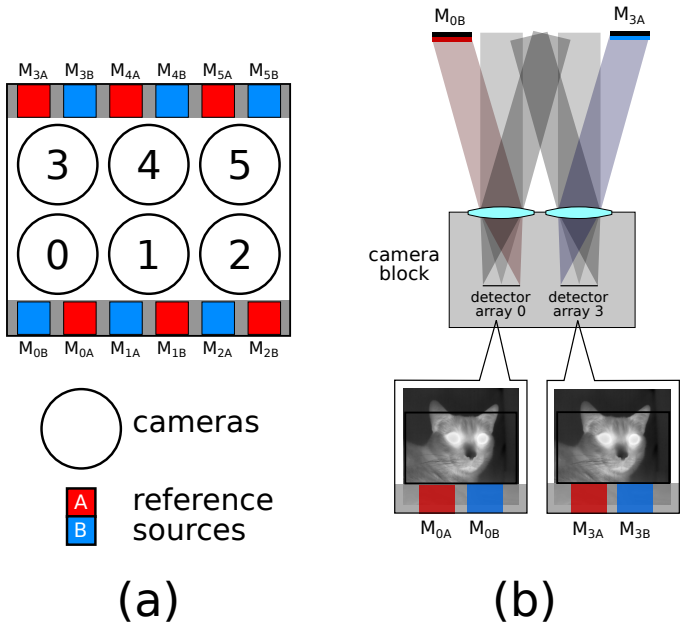

Figure 1: An example layout for a 2×3 array of cameras, using an array of 12 reference sources M_{ij} — one warm and one cool source for each camera i. (a) A view of the camera array, seen from the point of view of the object, in which the backs of the reference sources are made visible for clarity. (b) A cross-sectional view of the camera array and reference sources. The black border indicates the portion of the field of view that is unobstructed for all six cameras.

For a reference source placed a distance z in front of a camera lens of focal length f, the image will occur at a distance z' behind the lens, where

$$\frac{1}{z'} = \frac{1}{z} + \frac{1}{f} \,.$$

We will refer to z' as the "aperture location". Many microbolometer cameras use a rather short focal length, so that the object distance can be approximated as infinite. In this case, the defocus distance becomes $z' - f$, causing a point at the aperture to blur into a circle of radius $b_\mathrm{r} = (z' - f)/(2f_\#)$ for a lens with f-number $f_\#$. Using p for the pixel size of the detector, we can express the blur diameter in units of pixels as

$$b_\mathrm{d} = \frac{z' - f}{p f_\#} \,.$$

The blur diameter b_d gives the number of pixels in the image that we need to allow between the blurry edge of the aperture and the unblurred image of the reference source. For example, if we use a microbolometer camera with 25 µm pixels, and an $f_\# = 1.25$ lens of focal length $f = 9$ mm, then placing the aperture at a distance of 300 mm in front of the camera array will produce a blur margin of

$$b_\mathrm{d} = \frac{9.28\,\mathrm{mm} - 9\,\mathrm{mm}}{(2.5 \times 10^{-2}\,\mathrm{mm})(1.25)} = 9.0\,\mathrm{pixels} \,.$$

In general, we will want to have an extended region of pixels to view the reference blackbody sources. If we choose to image the sources into a 5×5 pixel region, and allow an error margin of an additional 2 pixels, then the aperture boundary will reduce the image size by 16 pixels in both the top and the bottom of the image, i.e. a loss of a total of 32 rows of data. If the detector array format used in our arrayed cameras are 320×256 format, then adding the aperture for dynamic calibration will cause a loss of $32/256 = 12.5\%$ of the overall image.

5. CONCLUSION

Although microbolometer thermal cameras are inexpensive in comparison to their cryo-cooled counterparts, they remain much more expensive than visible cameras, for the same number of pixels. There are a number of applications — snapshot

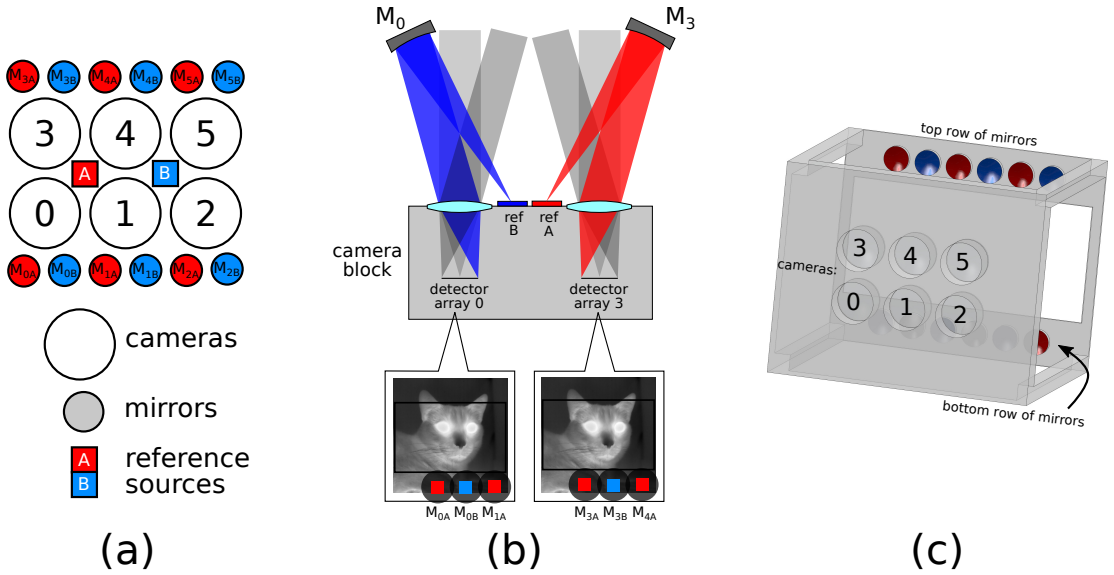

Figure 2: An example layout for a 2×3 array of cameras, using one cool and one warm reference source and an array of mirrors M_{ij}: two mirrors j for each camera i. (a) A view of the camera array, seen from the point of view of the object, in which the backs of the mirrors are made visible for clarity. (b) A cross-sectional view of the camera array and reference sources. The black border indicates the portion of the field of view that is unobstructed for all six cameras. (c) A 3D view of the mirror and camera lens array, as seen from a perspective behind the camera block. (The camera detector cores are not shown for clarity.)

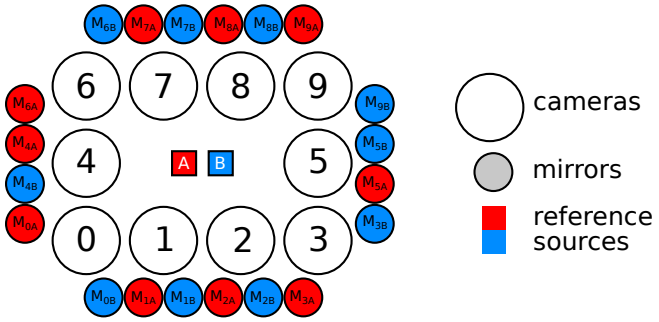

Figure 3: An example layout for dynamic calibration with a 10-camera array and 20 mirrors.

spectral[7] and polarization imaging[8] in particular — where the number of pixels is insufficient for doing useful work.[9] However, if we can use an array of cameras we can increase the number of pixels available without making extreme demands on detector manufacturers. For microbolometer cameras, however, radiometric matching between cameras has been a long-standing problem that has gotten in the way of doing this kind of array imaging. As we have shown above, by carefully designing an aperture to block the edge of the cameras' field of view, we can insert reference blackbody sources into the image of each camera and dynamically recalibrate them while collecting measurement data. This enforces radiometric matching between the cameras, opening up camera arrays to applications that have until now been blocked by the difficult problem of calibration drift. The tradeoff is a reduction in the available field of view.

In Figures 1 & 2, we show example layouts for an array of six cameras. Other layouts are of course possible, such as the 10-camera layout shown in Fig. 3. As the number of cameras in the array increases, however, parallax between the individual cameras' field of view becomes larger and more difficult to correct. In addition, if we use more than two rows of cameras in our array (such as the three rows used in Fig. 3, then we have to sacrifice pixels in the left and right sides of the fields of view and not just the top and bottom, if we want all of the cameras to have an overlapping field of view.

6. ACKNOWLEDGEMENTS

The original work for developing dynamic calibration hardware was done in 2014, while the author was employed at Rebellion Photonics, Inc., and the method was published in a series of patents.[10] Although I would have liked to make experimental data available to demonstrate the effectiveness of the technique, this has unfortunately not yet been made available.

REFERENCES

1. W. J. Parrish and J. T. Woolaway, "Improvements in uncooled systems using bias equalization," *Proc. SPIE* **3698**, 748–755 (1999).
2. P. W. Nugent, J. A. Shaw, and N. J. Pust, "Correcting for focal-plane-array temperature dependence in microbolometer infrared cameras lacking thermal stabilization," *Opt. Eng.* **52**, 061304 (2013).
3. K. Liang, C. Yang, L. Peng, and B. Zhou, "Nonuniformity correction based on focal plane array temperature in uncooled long-wave infrared cameras without a shutter," *Appl. Opt.* **56**, 884–889 (2017).
4. R. Olbrycht, B. Wiecek, and G. D. Mey, "Thermal drift compensation method for microbolometer thermal cameras," *Appl. Opt.* **51**, 1788–1794 (2012).
5. S. Chang and Z. Li, "Single-reference-based solution for two-point nonuniformity correction of infrared focal plane arrays," *Infrared Phys. & Technol.* **101**, 96–104 (2019).
6. D. L. Perry and E. L. Dereniak, "Linear theory of nonuniformity correction in infrared staring sensors," *Opt. Eng.*(8) **32**(8), 1854–1859 (1993).
7. N. Hagen and M. W. Kudenov, "Review of snapshot spectral imaging technologies," *Opt. Eng.*(9) **52**(9), 090901 (2013).
8. N. Hagen, S. Shibata, and Y. Otani, "Calibration and performance assessment of microgrid polarization cameras," *Opt. Eng.* **58**, 082408 (2019).
9. N. Hagen, R. T. Kester, C. Morlier, J. A. Panek, P. Drayton, D. Fashimpaur, P. Stone, and E. Adams, "Video-rate spectral imaging of gas leaks in the longwave infrared," *Proc. SPIE* **8710**, 871005 (2013).
10. R. T. Kester and N. Hagen, "Divided-aperture infra-red spectral imaging system" (2017–2019). US patents 9562849, 9599508, 10444070, 10254166, 10267686.